EurJOC
European Journal of Organic Chemistry

Full Papers
doi.org/10.1002/ejoc.202001661

Chemistry Europe
European Chemical Societies Publishing

Azaphilone Pigments from *Hypoxylon rubiginosum* and *H. texense*: Absolute Configuration, Bioactivity, and Biosynthesis

Kevin Becker,[a, b] Eric Kuhnert,[c, d] Russell J. Cox,[c, d] and Frank Surup*[a, b]

We report new stromatal azaphilone pigments rubiginosins Z-X from the ascomycete *Hypoxylon rubiginosum*, as well as rubiginosins Z and W from *H. texense*, which were isolated along with known monomeric and dimeric congeners. Structures were elucidated using comprehensive HRMS, NMR, and ECD analysis, revealing azaphilones from both fungi to be exclusively C-8(*S*)-configured. The orsellinic acid (OA)-carrying rubiginosins A, Z and dimeric rutilins A-B exhibited cytotoxicity. Rubiginosins X-W bearing linear polyketide side chains as well as rutilins A-B were antimicrobial. Structures of the differently-substituted azaphilones were linked to two putative biosynthetic gene clusters (BGCs; *hraza1/2*) in *H. rubiginosum*, which are proposed to collaboratively synthesize the OA-substituted azaphilones. These share high homology with the azaphilone-forming BGCs *hfaza1/2* from *H. fragiforme*. Comparison of *hraza* and *hfaza* suggests that lack of an FAD-dependent monooxygenase and acyltransferase gene in *hraza1* prevent formation of C-8(*R*)-configured fatty acid-substituted azaphilones in *H. rubiginosum*. The polyketide synthase-derived side chain of rubiginosins C and X-W is not encoded in the respective BGCs, showing that a third BGC is hypothetically involved in their formation. Cross-interaction of three BGCs which are forming a single molecule is unprecedented in fungal natural product biosynthesis.

Introduction

Azaphilones are a group of polyketide pigments produced by a large number of fungal species. Already described in 1931, the mycotoxin citrinin was the first representative of this class of secondary metabolites,[1] of which more than 600 members are known to-date.[2] All azaphilones share a pyronoquinone core, which undergoes a variety of modifications. The resulting structural diversity, in turn, leads to a large number of biological activities associated with azaphilones.[2b]

Among the known producers, the family Hypoxylaceae is distinguished for production of a large diversity of azaphilones in their stromata (fruiting bodies). Around 60 distinct compounds discovered to-date, *including* the orsellinic acid (OA)-carrying monomeric (+)-mitorubrins[3] and dimeric rutilins,[4] or the differentially substituted cohaerins,[5] lenormandins,[6] and daldinins.[7] The presence (or absence) and the structural architecture of azaphilones serve as a valuable chemotaxonomic tool for genus and species delimitation in the Hypoxylaceae. This is exemplified by the segregation of the genus *Jackrogersella* from *Annulohypoxylon* mainly due to the presence of cohaerin-type azaphilones in the latter.[8]

Recently, *Hypoxylon fragiforme*, the type species of the genus, was found to contain unusual fatty acid-carrying azaphilones named fragirubrins.[9] Moreover, unprecedented bisazaphilones termed hybridorubrins have been characterised, which constitute heterodimers of mitorubrin- and fragirubrin-type subunits. These dimers are likely produced by an interplay of biosynthetic pathways encoded on two separate and distantly-located biosynthetic gene clusters (BGCs), as identified by genome mining approaches.[10] Additionally, the observed presence of subclasses with opposite C-8 configurations could be ascribed to the presence of two different FAD-dependent monooxygenases.[9b] Interestingly, a recent systematic genome-mining study of high-quality genomes from Hypoxylaceae species revealed *H. rickii* to also carry two azaphilone BGCs, while other relatives such as *H. pulicicidum* and *J. multiformis* only contain a single cluster.[11]

Hypoxylon rubiginosum, in turn, is another frequently encountered species of the genus that occurs in temperate regions of the northern hemisphere.[12] It typically produces OA-carrying rubiginosins A **1** and B **2**, as well as the linear polyketide-substituted rubiginosin C **3**. These secondary metabolites were first described from stromata of *H. rubiginosum* in addition to the known mitorubrins.[13] The linear polyketide

[a] *K. Becker, Dr. F. Surup*
Department Microbial Drugs
Helmholtz Centre for Infection Research GmbH (HZI)
Inhoffenstraße 7, 38124 Braunschweig, Germany
E-mail: frank.surup@helmholtz-hzi.de
[b] *K. Becker, Dr. F. Surup*
German Centre for Infection Research Association (DZIF)
Partner site Hannover-Braunschweig
Inhoffenstraße 7, 38124 Braunschweig, Germany
[c] *Dr. E. Kuhnert, Prof. Dr. R. J. Cox*
Institute for Organic Chemistry, Leibniz University Hannover
Schneiderberg 1B, 30167 Hannover, Germany
[d] *Dr. E. Kuhnert, Prof. Dr. R. J. Cox*
Centre for Biomolecular Drug Research (BMWZ)
Schneiderberg 38, 30167 Hannover, Germany

Supporting information for this article is available on the WWW under https://doi.org/10.1002/ejoc.202001661

moiety of **3**, rubiginosic acid, has furthermore been isolated from stromatal extracts as a free acid.[13] Mycelial cultures of *H. rubiginosum* are currently under investigation as biocontrol agents against the ash dieback pathogen *Hymenoscyphus fraxineus* due to antagonistic effects that are probably mediated in part through the production of phomopsidin and related polyketides.[14]

In an effort to assess the diversity of rubiginosin-type azaphilones in the Hypoxylaceae, we investigated collections of *H. rubiginosum* and the related *H. texense*[15] for known and novel azaphilones. Additionally, we strived to complement missing stereochemical assignments and supply more bioactivity data on the monomeric rubiginosins A-C **1**–**3** and dimeric rutilins A-B **9**–**10**. Availability of a genome sequence of *H. rubiginosum*[10] enabled us to identify the putative biosynthetic gene clusters (BGCs) for azaphilone formation and to propose a coherent biosynthetic scheme.

Results and Discussion

Isolation and structure elucidation

Stromata of *Hypoxylon rubiginosum* and *H. texense* were collected from dead wood in Europe and North America, respectively. Extraction followed by gradual preparative chromatography yielded the pigments **1**, **3**–**7**, **9**–**10**, and **13** (Figure 1). Their structures were solved by NMR analysis (Tables S1–S2, Figures S3–S33) aided by electronic circular dichroism (ECD) measurements (Figure S34). Among the isolated compounds, rubiginosin Z **4** was isolated as a natural product for the first time, while rubiginosins Y-W **5**–**7** comprise unprecedented structures.

Confusingly, unrelated meroterpenoids isolated from the plant *Rhododendron rubiginosum* have also been named rubiginosins A-G.[16] In order to avoid further confusion the new compounds described here are named rubiginosins Z-W to maintain consistency with the related *H. rubiginosum* compounds first described in 2004.[13]

HPLC-UV/vis chromatograms of the crude extracts, along with the corresponding source of substances, is given in Figure S1. Two chemotypes (CTs) of *H. rubiginosum* were analysed: CT-1 contains rubiginosins A **1** and C **3** as reported,[17] along with rubiginosin Z **4**, mitorubrinol acetate **13**, and orsellinic acid (OA, **14**) in large amounts. Moreover, traces of rubiginosin Y **5**, rutilins A-B **9**–**10**, and mitorubrinol **12** were detected. CT-2, also termed "aberrant", contained **6** instead of **3** and **5**, but was otherwise similar. Stromata of *H. texense* were found to contain **1**, **4**, and **13** as major constituents. Besides, rubiginosin B **2**, entonaemin A **8**, rubiginosin W **7**, rutilins A-B **9**–**10**, and **14** were also observed.

Rubiginosin Z **4** was shown to have a molecular formula (MF) of $C_{23}H_{24}O_9$ by HR-ESI-MS analysis (*cf.* Figure S2). The ^1H and ^{13}C NMR data (Figures S3–S8) confirmed **4** to be the acetylated congener of rubiginosin B **2** previously obtained by chemical derivatisation.[13] Accordingly, this is the first description of **4** as a natural product. Derivatization of **4** using Mosher's method[18] revealed the absolute configuration to be C-8(*S*). This was supported by electronic circular dichroism (ECD) analysis of **4** (Figure S34) in comparison with ECD spectra of synthetically

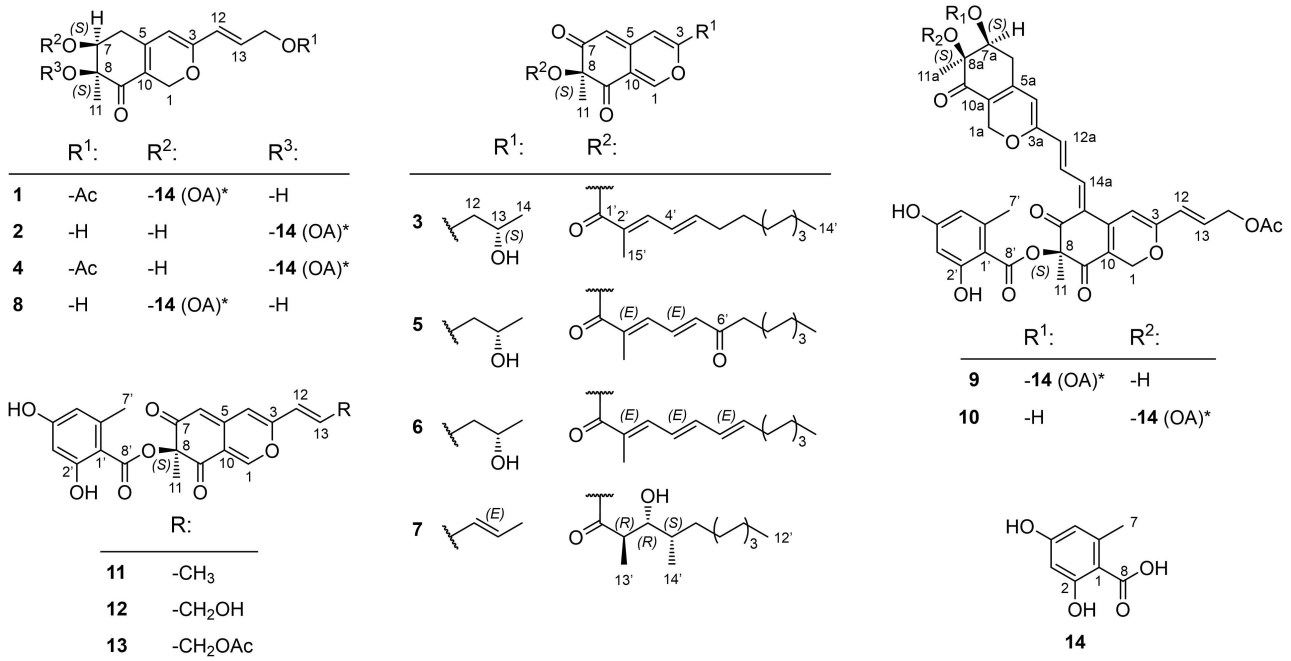

Figure 1. Structures of novel (**4**–**7**) and known (**1**–**3**, **8**–**13**) azaphilone natural products, as well as orsellinic acid (OA, **14**) from stromata of *Hypoxylon rubiginosum* and *H. texense.* **1**–**3**: rubiginosins A-C, **4**–**7**: rubiginosins Z-W, **8**: entonaemin A, **9**–**10**: rutilins A-B, **11**: mitorubrin, **12**: mitorubrinol, **13**: mitorubrinol acetate, **14**: orsellinic acid (OA). Rubiginosin Z **4** was only obtained by chemical derivatisation before. * OA is esterified to the azaphilone backbone *via* its C-8.

prepared azaphilone stereoisomers.[19] The positive Cotton effects (CEs) of **4** at *ca.* 340 nm and the negative CE at *ca.* 295 nm were also in accordance with the C-8(*S*)-isomer. Furthermore, the occurrence of positive polarization in **4** confirmed this assignment. Taking ^{1}H/^{1}H ROESY correlations into account (Figure 2), the relative *syn*-configuration of 7-H and 11-H$_3$ was confirmed,[13] showing that C-7 is also (*S*)-configured.

Rubiginosin Y **5**, which was only detected in *H. rubiginosum*, was shown to possess a MF of $C_{28}H_{36}O_7$ by HR-ESI-MS analysis. By examining its NMR spectra (Figures S9–S14), a high overall similarity to rubiginosin C **3** was observed.[13] The only difference between **5** and **3** was occurrence of a C-6′ ketone in **5**. This was confirmed by its chemical shift ($\delta_{C\text{-}6'}$ = 200.4 ppm), as well as ^{1}H/^{13}C HMBC correlations from the neighbouring protons 4′-H, 5′-H, 7′-H$_2$, and 8′-H$_2$ (Figure 2).The alkene configurations of $\Delta^{2',3'}$ and $\Delta^{4',5'}$ were assigned as *E* due to ^{1}H/^{1}H ROESY correlations of 15′-H$_3$/4′-H and 3′-H/5′-H (Figure 2). For **5**, a C-8(*S*)-configuration was determined by analysis of ECD data (Figure S34).[19] A positive CE was observed at *ca.* 350 nm, while negative CEs were monitored at *ca.* 270–290 nm. This matches with ECD spectra taken for rubiginosin C **3**, which was reported to be C-8(*S*)-configured.[13]

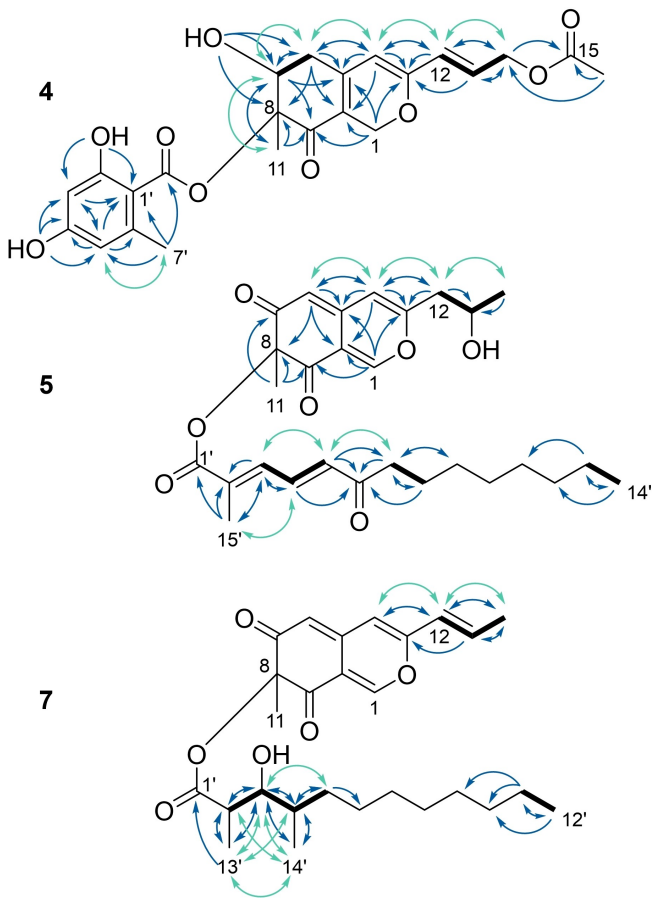

Figure 2. Key NMR correlations of rubiginosins Z-Y **4**–**5** and W **7**. Bold bonds: ^{1}H/^{1}H COSY correlations; solid, blue arrows: ^{1}H/^{13}C HMBC correlations; solid, turquoise arrows: ^{1}H/^{1}H ROESY correlations. Redundant NMR correlations in **7** as compared to **5** were omitted.

Rubiginosin X **6** from *H. rubiginosum*, for which HR-ESI-MS analysis revealed a MF of $C_{28}H_{36}O_6$, was established in a similar manner as **5**. The key difference was the unsaturation of C–6′/C–7′ in **6** as compared to **3**, which resulted in a total of three conjugated alkenes in the polyketide chain. The configurations of $\Delta^{2',3'}$, $\Delta^{4',5'}$, and $\Delta^{6',7'}$were assigned as *E* due to ^{1}H/^{1}H ROESY correlations of 15′-H$_3$/4′-H, 3′-H/5′-H, 4′-H/6′-H, and 5′-H/7′-H, respectively. The stereocenter C-8(*S*) was solved by matching ECD data of **6** with **3** and **5** (Figure S34). C-13(*S*) was conferred from Mosher analysis of **3** due to a shared biosynthesis.[20]

Rubiginosin W **7** was exclusively detected in (and thus isolated from) *H. texense* and found to have a MF of $C_{27}H_{38}O_6$ by HR-ESI-MS. It was found to possess the same general azaphilone core as **3** and **5**–**6**. Positive optical rotations and matching ECD data (Figure S34) suggested **7** to share the same C-8(*S*)-configuration as **1**–**6**. However, a differing C-12 to C-14 moiety and linear polyketide chain were deduced from NMR data. The former was shown to be a 1-propene residue due to ^{1}H/^{13}C HSQC data and ^{1}H/^{1}H COSY correlations between 12-H, 13-H, and 14-H$_3$ (Figure 2). The geometry of $\Delta^{12,13}$ was deduced to be *E* from its coupling constant ($^{3}J_{12\text{-}H,13\text{-}H}$ = 15.6 Hz). The polyketide was shown to be a saturated C_{12} chain, as compared to the polyunsaturated C_{14} unit found in **3** and **5**–**6**. In **7**, ^{1}H/^{13}C HMBC correlations from 13′-H$_3$ to C-1′, C-2′, and C-3′, from 14′-H$_3$ to C-3′, C-4′, and C-5′, as well as the chemical shift of C-3′ (δ_C = 75.6 ppm) indicated a 2′,4′-dimethyl-3′-ol substructure. The methyl terminus was established by ^{1}H/^{13}C HMBC correlations from 12′-H$_3$ to C-11′ and C-10′. The remaining carbons C-7′ to C-9′ were placed in between.

The absolute configuration of C-3′ in **7** was deduced by applying Mosher's method.[18] The $\Delta\delta_{S,R}$ of 2′-H was found to be zero and that of 13′-H$_3$ was negative. In turn, the $\Delta\delta_{S,R}$-values of protons 4′-H, 5′-H$_2$, and 14′-H$_3$ were uniformly positive. Thus the absolute configuration of C-3′(*R*) was deduced.

To solve the absolute configurations of C-2′ and C-4′, their configurations relative to C-3′(*R*) were solved using ^{1}H/^{1}H ROESY correlations and a *J*-based conformational analysis (Figure 3; *cf.* Figure S35 for all possible rotamers).[20] The *J*-values were extracted from *J*-resolved ^{1}H/^{13}C HMBC[21] and ^{1}H/^{13}C HSQC HECADE[22] spectra (Figures S27–S30). According to the original publication, the *J*-values were assigned the descriptors "large" and "small".[20]

For the C-2′/C-3′ bond, a $^{3}J_{2'\text{-}H,3'\text{-}H}$ of 8.4 Hz indicated an *anti*-orientation of 2′-H and 3′-H. Moreover, ^{1}H/^{1}H ROESY correlations between 13′-H$_3$/3′-H, 13′-H/4′-H, 13′-H/14′-H$_3$, and 2′-H/14′-H$_3$ were observed, implying a *gauche*-orientation of both methyls C-13′ and C-14′. This was supported by small coupling constants of $^{3}J_{2'\text{-}H,C'\text{-}4}$ (1.9 Hz), $^{3}J_{3'\text{-}H,C'\text{-}1}$ (2.6 Hz), and $^{3}J_{3'\text{-}H,C'\text{-}13}$ (2.1 Hz), indicating respective *gauche*-orientations. Furthermore, the large $^{2}J_{2'\text{-}H,C'\text{-}3}$ of −5.1 Hz implied a *gauche*-orientation of 2′-H and 3′-OH. This showed the C-2′/C-3′ configuration to be *erythro*. Taking the C-3′(*R*)-configuration into account, C-2′(*R*) was derived.

Similarly, the relative configuration of the C-3′/C-4′ bond was solved. The $^{3}J_{3'\text{-}H,4'\text{-}H}$ of 3.3 Hz indicated a *gauche*-orientation of 3′-H and 4-H′. In addition, ^{1}H/^{1}H ROESY correlations between 3′-H/4′-H, 3′-H/5′-H$_2$, 4′-H/13′-H$_3$, 13′-H$_3$/14′-H$_3$, as well as 2′-H/

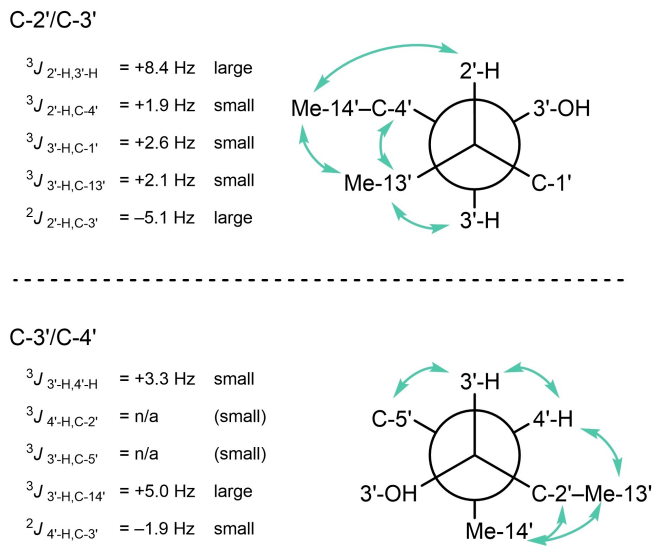

Figure 3. Newman projections of *assigned* rotamers from C-C bonds in rubiginosin W **7** used for a *J*-based assignment of relative stereochemistry.[20] Experimental *J*-values and assigned descriptors (small/large) are depicted. Plain, turquoise arrows: Observed ^{1}H/^{1}H ROESY correlations. Values for $^3J_{4'\text{-H},C\text{-}2'}$ and $^3J_{3'\text{-H},C\text{-}5'}$ could not be extracted from the NMR spectra. All twelve hypothetical rotamers are depicted in Figure S35.

14′-H$_3$ were observed, again indicating a *gauche*-orientation of C-13′ and C-14′. The $^3J_{3'\text{-H},C\text{-}14'}$ of 5.0 Hz indicated an *anti*-orientation of 3′-H and C-14′. The $^2J_{4'\text{-H},C\text{-}3'}$ of −1.9 Hz showed that 4′-H and 3′-OH are also *anti*. Taken together, this indicated the C-3′/C-4′ bond to be *threo*. Taking C-3′(*R*) into account, C-4′(*S*) was derived. Ultimately, the polyketide chain of **7** was found to be (2*R*,3*R*,4*S*)-3-hydroxy-2,4-dimethyl-dodecanoic acid, which was in accordance with NMR data of a synthetically-obtained enantiomer (Table S3).[23]

For the known azaphilones **1**, **3**, **9**–**10**, and **13**, comparison of NMR, optical rotation, and ECD data with respective references resulted in the following assignments: rubiginosins A **1** and C **3**,[13] rutilins A-B (**9**–**10**),[4] and (+)-mitorubrinol acetate **13**.[3] The occurrence of **9**–**10** in *H. rubiginosum* and *H. texense* (*cf.* Figure S1) has not been reported before, as these azaphilones had only been described from *H. rutilum*.[4] Previously missing stereochemical assignments of the known **1**, **3**, **9**–**10** are complemented in the following paragraphs.

The stereocenter C-8 in **1** is a tertiary alcohol and thus cannot be analysed with Mosher's method. However, ^{1}H/^{1}H ROESY correlations of 7-H and 11-H$_3$ indicated a *syn*-conformation as previously observed in **4**.[13] Congruent ECD data of **1** and **4** with positive CEs at 223, 262, and 335 nm as well as negative CEs at 244 and 295 nm (Figure S34) confirmed the C-7(*S*)/C-8(*S*)-configuration of **1**. Positive optical rotations of **1** and **4** supported these results. This was further under-pinned by biosynthetic considerations (see respective section below). These results can be extended to rubiginosin B **2** and entonaemin A **8**, for which positive optical rotations of $[\alpha]_D^{25} = +21$[13] and $[\alpha]_D^{25} = +132$[24] were reported, respectively. For **8**, this value was reported from a *Talaromyces* sp. that also produced (+)-mitorubrin, but not from the original producer of **8**, *Entonaema*, which is from the same family as *Hypoxylon*.

For the dimeric rutilins A-B **9**–**10**, the relative *syn*-configuration of C-7a/C-8a was deduced in a similar manner *via* ^{1}H/^{1}H ROESY correlations as described above. We hypothesize a similar dimerization reaction to take place as proposed for the hybridorubrins (Figure S36).[9b] However, the connectivity is inverted: while hybridorubrins consists of a northern mitorubrin- and a southern fragirubrin moiety, **9**–**10** comprise a northern rubiginosin- and a southern mitorubrin-type unit. Hence, biosynthesis of **9**–**10** is proposed to link mitorubrinol acetate **13** to aldehyde derivatives of **8** and **2**, respectively. In this mechanism (Figure S36), the C-14 hydroxy moieties of **8** and **2** are oxidized to form aldehyde analogues, which, in turn, are nucleophilically attacked by the double bond $\Delta^{5,6}$ of **13** after rearrangement within the azaphilone core. This links both building blocks and forms a pyrilium ion. A subsequent water elimination *via* an E1cB mechanism and reduction of the pyrilium ion yields the respective dimers **9**–**10**. Following this hypothesis, the stereochemistry of **9**–**10** at C-7a(*S*), C-8(*S*), and C-8a(*S*) can be assigned due to their (*S*)-configured biosynthetic building blocks.

To conclude, by utilisation of ECD spectroscopy, optical rotation measurement, and comprehensive NMR analysis, it was shown that all azaphilones from *Hypoxylon rubiginosum* as well as *H. texense* share the same C-8(*S*) backbone stereochemistry, and, where applicable, C-7(*S*). This was further supported by analysis of the biosynthetic gene clusters (BGCs) responsible for azaphilone formation in *H. rubiginosum* (see Biosynthesis Section for details).

Bioactivity assessment

The bioactivities of **1**, **3**–**4**, **6**–**7**, **9**–**10**, and **13** were examined in two assays as described in the methods section. Evaluation of the cytotoxic activities of the isolated azaphilones against mammalian cell lines (Table 1) was initially conducted against murine fibroblasts (L929) and human endocervical adenocarcinoma cells (KB 3.1). For **1**, **4**, and **9**–**10**, half-maximum inhibitory concentrations (IC_{50}) with values smaller than 10 μM were measured. Thus, five additional human cell lines were tested. For the monomeric, OA-carrying **1** and **4**, activity against all cell lines was observed with IC_{50} values of 0.3–14.9 μM. The OA-carrying **13** did not show any cytotoxicity as reported before,[9b] suggesting an influence of the OA moiety's position and/or occurrence of the C-7 ketone. The polyketide chain-carrying azaphilones **3** and **6**–**7** did not show cytotoxic activities, except for weak activity of **6** against KB 3.1. This indicates that presence of the OA moiety has a strong influence on cytotoxicity in contrast to a linear polyketide unit. Similarly, the fatty acid-carrying fragirubrins were also absent of cytotoxic effects.[9b] The dimeric rutilins A-B **9**–**10** showed the strongest cytotoxicity among the tested compounds with IC_{50} values of 0.3–2.9 and 0.2–1.1 μM, respectively. In comparison, the known dimeric azaphilones rutilins C-D from *Hypoxylon fragiforme* did not exhibit cytotoxic effects.[9b] Rutilins C-D consist of two

Table 1. Results of the cytotoxicity assessment of rubiginosins A, C, Z, X-W (**1**, **3**, **4**, **6**–**7**), rutilins A-B (**9**–**10**), and mitorubrinol acetate (**13**). Cytotoxic activities were measured as half-maximum inhibitory concentrations (IC_{50}). Compound **5** was not tested due to lack of material, while **2** and **8** were not isolated in this work. (–): no cytotoxicity observed. Empty cell: not tested.

cell line		IC_{50} [μM]								
		1	**3**	**4**	**6**	**7**	**9**	**10**	**13**	ref.[a]
L929	mouse fibroblasts	3.2	–	4.7	–	–	1.2	0.6	–	0.000031
KB 3.1	human endocervical adenocarcinoma (AC)	5.2	–	5.2	29.9	–	1.0	0.7	–	0.000028
PC-3	human prostate AC	5.2		5.6			0.9	0.3		0.000140
SK-OV-3	human ovary AC	5.2		5.4			0.6	0.3		0.000120
MCF-7	human breast AC	0.3		1.2			0.3	0.2		0.000026
A-431	human squamous AC	2.0		5.9			0.3	0.2		0.000026
A-549	human lung carcinoma	14.9		12.8			2.9	1.1		0.000042

[a] Epothilone 1.0 mg/mL.

mitorubrin-type building blocks, while **9**–**10** are dimers of one mitorubrin and one rubiginosin-type moiety. As the monomeric **1** and **4** exhibited cytotoxicity while the mitorubrins did not,[9b] the strong cytotoxicity of the dimeric rutilins **9**–**10** can be putatively ascribed to the rubiginosin-type unit.

The antimicrobial activities of **1**, **3**–**4**, **6**–**7**, **9**–**10**, and **13** were assessed as minimum inhibitory concentrations (MICs) against various bacterial and fungal test organisms (Table S4). The group of monomeric, orsellinic acid (OA)-carrying **1**, **4**, and **13** did not show any inhibition of microbial growth, regardless of the substituent's position (C-7 *vs.* C-8). For **13**, this is in agreement with previous data,[9b] while for **1**, weak antimicrobial activities were reported.[25] The monomeric, polyketide chain-carrying rubiginosins **3** and **6**–**7**, however, showed weak antibacterial activities against *Bacillus subtilis* and *Staphylococcus aureus*. Furthermore, **3** and **6** exhibited a weak antifungal effect against *Rhodotorula glutinis*. In turn, no antimicrobial activities were reported for the related, fatty acid-carrying fragirubrins,[9b] indicating an influence of the C-8 and/or C-3 substituent on antimicrobial activity. Curiously, the dimeric rutilin A **9** showed the strongest activity with an MIC of 1 μg/mL against *B. subtilis*, while rutilin B **10** did not exhibit any activity against this organism. These MICs were confirmed by independent assay replication and indicate a strong influence of the OA position. Moreover, weak MICs against *S. aureus* were measured for **9** and **10**. Against *Escherichia coli* **9** exhibited weak activity, while **10** showed weak antifungal effects against *Mucor hiemalis*. Rutilins C and D showed no antimicrobial activity in the same assays,[9b] further demonstrating the importance of the OA moiety's position. Eventually, more congeners will need to be assessed to allow for deduction of structure-activity relationships (SARs). In turn, this will be necessary to deduce the molecular targets of these azaphilone compounds.

In summary, the diversity of azaphilones produced by *H. rubiginosum* and *H. texense* covers a broad range of biological activities which are potentially beneficial for the survival and distribution of the fungus. Thus, they might explain why the highly energy-consuming azaphilone production and diversification is maintained in stromata across various lineages of the Hypoxylaceae.

Biosynthesis of azaphilones in *H. rubiginosum*

We previously sequenced the genome of the ex-epitype strain of *H. rubiginosum* (MUCL 52887),[10] enabling us to perform genome mining for the identification of the azaphilone biosynthetic genes. In a previous study we already identified the mostly likely pathway for azaphilone biosynthesis in *H. fragiforme*,[9b] which is a well-known producer of mitorubrins. Therefore, it is likely that *H. rubiginosum* contains similar biosynthetic gene clusters (BGCs). BLASTp searches using the protein sequences of the polyketide synthase (PKS) core enzymes from the mitorubrin pathway in *H. fragiforme* (Hfaza1A and Hfaza2A) against an *H. rubiginosum* protein database quickly revealed homologues in the latter with high similarity (74 and 77%, respectively). These two homologous clusters in *H. rubiginosum* (*hraza1* and *hraza2*; Figure 4) are located on separate scaffolds. Each PKS gene is clustered with a set of tailoring genes.

To validate if both clusters are putatively involved in the azaphilone biosynthesis of *H. rubiginosum*, a homology analysis with the *hfaza1* and *hfaza2* BGCs from *H. fragiforme* was conducted using the clinker tool (Figure 4).[26] The analysis revealed the candidate BGCs from *H. rubiginosum* to be highly similar in gene content as well as gene arrangement to those from *H. fragiforme*.

Manual searches for other PKS genes in the genome of *H. rubiginosum* showed the presence of at least 38 additional BGCs, however, none of them contained the necessary genes for azaphilone biosynthesis. Thus, the two identified BGCs are likely involved in the biosynthesis of azaphilones in *H. rubiginosum* and were designated as *hraza1* and *hraza2*. The *hraza* genes were labelled in accordance with those associated with the *hfaza1* and *hfaza2* clusters.[9b] While the cluster pair *hraza2* and *hfaza2* is identical (except for the presence of the gene *hraza2N* with unknown function), *hraza1* differs from *hfaza1* by the lack of homologues of the FAD-dependent monooxygenase Hfaza1D and the acyltransferase Hfaza1E. Both enzymes are associated with a branching point in the *H. fragiforme* azaphilone pathway leading to a variety of fatty acid-linked azaphilones (lenormandins, fragirubrins) with opposite C-8(*R*)-configuration compared to the C-8(*S*) mitorubrins.[9b] The lack of the respective genes in *H. rubiginosum* corresponds well with

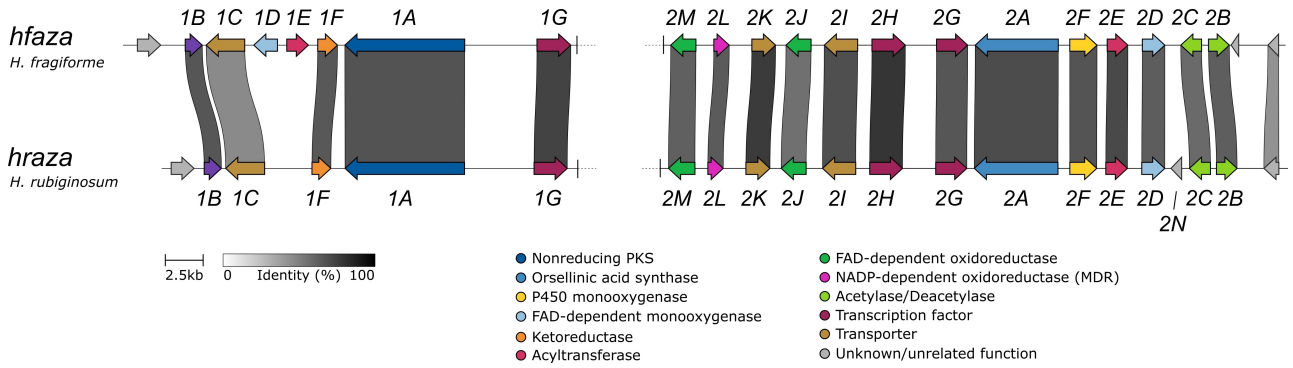

Figure 4. Comparison of the biosynthetic gene clusters (BGCs) encoding for azaphilone production in *H. fragiforme* (*hfaza1/2*) and *H. rubiginosum* (*hraza1/2*) based on protein similarities visualized with the clinker tool.

the absence of fatty acid-linked azaphilones in this organism and a conserved C-8(*S*) stereochemistry independent of the attached side chain.

Azaphilones isolated from *H. rubiginosum* can be assigned to three types, which differ mainly in the position and structure of the attached side chain. While the biosynthesis of the mitorubrin-type **11**–**13** (type A) must be homologous to those reported in *H. fragiforme*, the pathway for rubiginosin A **1** and entonaemin A **8** (type B) is less clear and cannot be ascribed to the lack of Hfaza1D and Hfaza1E homologues. In both molecules, as well as in rubiginosin B **2**/Z **4**, a reduction step at the C-7 ketone is required to form an alcohol, which serves as a functional group for the ester bond formation with orsellinic acid **14**. As **1**–**2**, **4**, and **8** are not produced by *H. fragiforme*, an oxidoreductase encoded outside of the cluster might be responsible for this reduction, or possibly one of the encoded oxidoreductases is not functional in *H. fragiforme*. The position of the OA moiety could be result of non-specific activity of the acyltransferase Hraza2E or caused by a spontaneous transesterification reaction between the C-8 and C-7 position.

As we observed slow conversion of **4** to **1** and **10** to **9** (but not *vice versa*) under storage conditions over a period of months (Figure S37), ester bond formation at C-8 position by Hraza2E and subsequent spontaneous transesterification is more likely. In the case of **1** and **4**, molecular modelling studies (semi-empirical, PM3) suggest that **1** is *ca.* 11 kJ/mol lower in energy than **4** in agreement with the observed transfer of the *O*-orsellinoyl group from C-8 to C-7 (Figure S38). Calculation of low energy conformers showed that in **4**, the C-11 methyl takes up an unfavoured *pseudo*-axial position, while in **1** it adopts a less hindered *pseudo*-equatorial conformation (Figure S38). These results also explain why the reaction is apparently not reversible. To summarise, the observed transesterification reactions as well as biosynthetic considerations show that **4** and **10** (and **2** for that matter) are the actual final products of the azaphilone biosynthetic machinery in *H. rubiginosum*. This, in turn, renders **1** and **9** (also **8**) as by-products.

Type C azaphilones in *H. rubiginosum* are characterized by a PKS-derived side chain as observed for rubiginosin C **3** and Y-X **5**–**6**. In case of **3**, its free acid (rubiginosic acid) was even isolated from stromatal extracts.[13] Based on the structure of this side chain a highly-reducing (hr-)PKS with KS-AT-DH-C-MeT-ER-KR-ACP domain composition is likely to be the responsible biosynthetic core enzyme. Analysis of the proximities of the *hraza1/hraza2* clusters revealed the presence of a single hrPKS copy close to *hraza1*, which, however, lacked a complete methyltransferase domain. As the genome of *H. rubiginosum* contains 14 PKS genes with the proposed domain structure the origin of the side chain cannot yet be traced with the available bioinformatic tools. Even though the PKS for side chain formation cannot be identified yet, it seems more likely that the corresponding gene is located on a different genomic locus implying that three BGCs are putatively involved in the production of **3**, and **5**–**6** in *H. rubiginosum*. To the best of our knowledge, the interaction of three separate BGCs to create a natural product is unprecedented in fungi, but requires further experimental evidence.

Ester bond formation of the polyketide side chain with the azaphilone core scaffold is putatively also accomplished by Hraza2E which must have a rather broad substrate tolerance. As rubiginosic acid was never observed in *H. fragiforme* stromatal extracts, it is likely that the respective cluster is not present in this fungus or is not expressed during stromatal formation explaining the lack of type C azaphilones in *H. fragiforme*. Based on the previously proposed pathway for azaphilone diversification in *H. fragiforme* and the identified BGCs *hraza1* and *hraza2*, a scheme for the diversification of these compounds in *H. rubiginosum* can be given (Scheme 1).

Conclusion

We report the isolation and characterisation of the novel azaphilone natural products rubiginosins Z-X **4**–**6** from *Hypoxylon rubiginosum* as well as rubiginosins Z **4** and W **7** from *H. texense*. While **4** is the C-8 orsellinoyl isomer of rubiginosin A **1**, the novel **5**–**7** are congeners of the polyketide-carrying rubiginosin C **3**. Their absolute configurations were solved using comprehensive NMR studies including Mosher's analysis. In **7**, a *J*-based configurational assignment was utilised to solve the

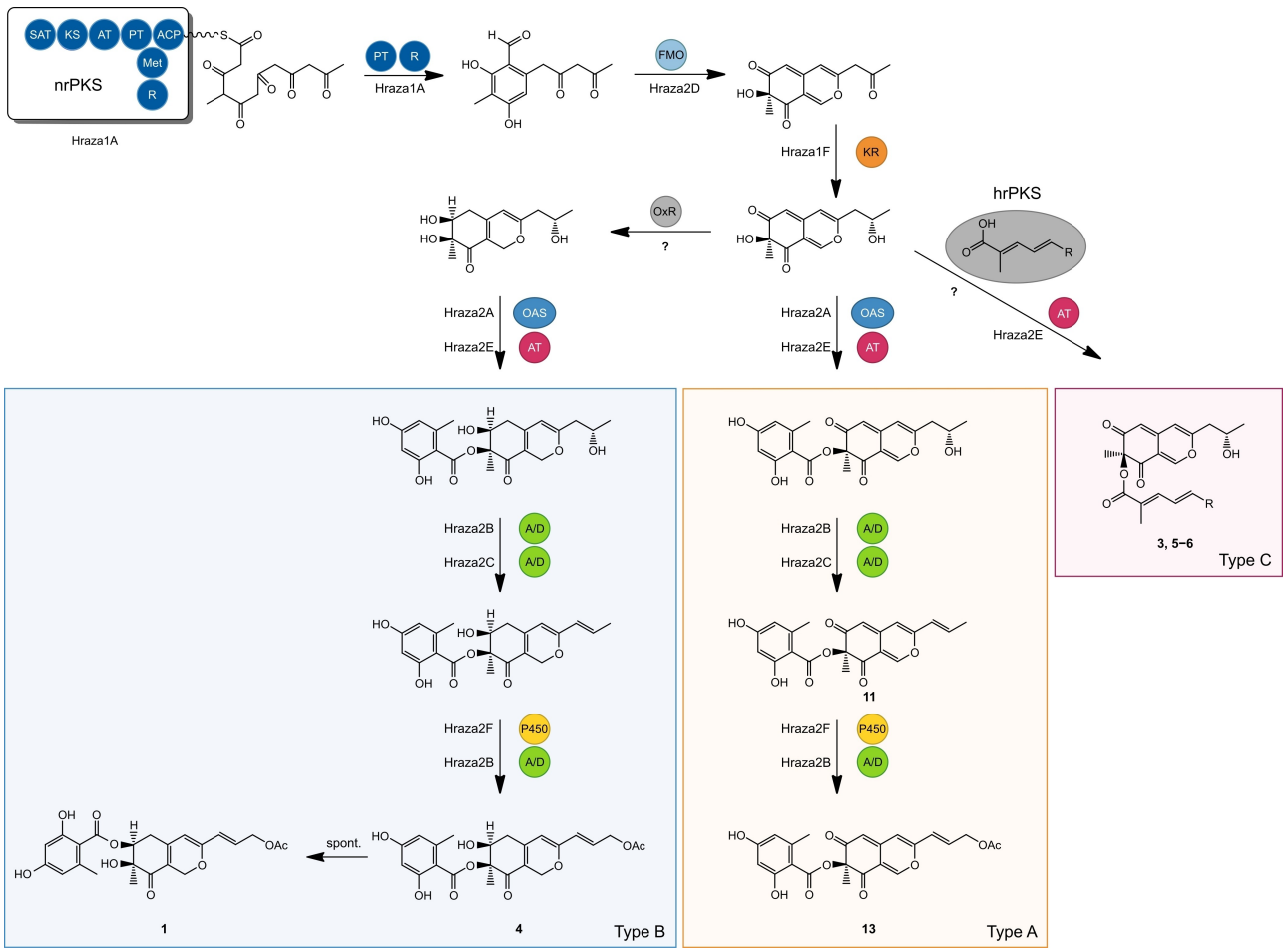

Scheme 1. Biosynthetic scheme for the formation of monomeric azaphilones by the *hraza1/2* biosynthetic gene clusters (BGCs) in *H. rubiginosum*. **nrPKS**: non-reducing polyketide synthase, **hrPKS**: highly-reducing polyketide synthase, **FMO**: FAD-dependent monooxygenase, **KR**: ketoreductase, **OxR**: oxidoreductase, **OAS**: orsellinic acid synthase, **AT**: acyltransferase, **A/D**: acetylase/deacetylase, **P450**: P450 monooxygenase. **1**: rubiginosin A, **3**: rubiginosin C, **4**–**6**: rubiginosin Z-X, **11**: mitorubrin, **13**: mitorubrinol acetate.

configurations of three consecutive stereocenters. We also clarified the absolute configurations of known rubiginosin and rutilin-type azaphilones.

According to HPLC-MS data and molecular modelling results, the major stromatal constituent **1** is a transesterification product of its *O*-8 isomer **4**. The same interconversion from *O*-8 to *O*-7 isomers was observed for the dimeric rutilins B **10** to A **9**, which contain a rubiginosin building block and were not yet reported from *H. rubiginosum* or *H. texense*. This reaction renders **4** and **10** the actual biosynthetic end products, and **1** and **9** by-products of spontaneous transesterification.

Representatives of the rubiginosins and rutilins were assessed for their antimicrobial and cytotoxic activities. The polyketide chain-carrying rubiginosins **3** and **5**–**6** showed weak antibacterial effects. The OA-bearing **1** and **4**, in turn, exhibited cytotoxicity against a variety of mammalian cell lines, while mitorubrin-type azaphilones were found to be devoid of activity. Moreover, the dimeric **9** showed a significant antibacterial activity against *Bacillus subtilis*, while its congener **10** showed no effect on this organism.

By genome mining, we identified two biosynthetic gene clusters (BGCs, *hraza1* and *hraza2*) which can explain the diversity of OA-esterified azaphilones in *H. rubiginosum*. In contrast, the production of the polyketide sidechain from **3** and **5**–**6** is not encoded by *hraza1* and *hraza2*, thus a third unidentified BGC is hypothesised to be involved. Accordingly, this is the first example of fungal natural products being synthesized by the interaction of three distantly located BGCs, but further experiments are needed for verification. The high similarity of *hraza1/2* with the *hfaza1/2* azaphilone BGCs from *H. fragiforme* gives insight into the evolution of azaphilone diversity, where *H. fragiforme* supposedly acquired an additional copy of an FAD-dependent monooxygenase and acyltransferase which led to the formation of fatty acid substituted azaphilones with opposite stereoconfiguration at C-8.

Experimental Section

General

NMR spectra were recorded with an Avance III 700 spectrometer with a 5 mm TCI cryoprobe (^{1}H 700 MHz, ^{13}C 175 MHz) and an Avance III 500 spectrometer (^{1}H 500 MHz, ^{13}C 125 MHz; both Bruker, Billerica, MA/USA). NMR data were referenced to selected chemical shifts of acetone-d_6 (^{1}H: 2.05 ppm, ^{13}C: 29.32 ppm), pyridine-d_5 (^{1}H: 7.22 ppm, ^{13}C: 123.87 ppm) and $CDCl_3$ (^{1}H: 7.27 ppm, ^{13}C: 77.00 ppm), respectively. Optical rotations were taken with a MCP 150 polarimeter (Anton Paar, Graz, Austria) and IR spectra using a Spectrum 100 FT-IR spectrometer (Perkin Elmer, Waltham, MA/USA). UV spectra were taken with a UV-2450 UV/vis spectrophotometer (Shimadzu, Kyoto, Japan), while ECD spectra were collected with a JD-815 spectrophotometer (Jasco, Pfungstadt, Germany)

ESI-MS spectra were recorded with an UltiMate® 3000 Series uHPLC (Thermo Fisher Scientific, Waltman, MA/USA) utilizing a C18 Acquity® UPLC BEH column (2.1×50 mm, 1.7 μm; Waters, Milford, MA/USA) connected to an amaZon® speed ESI-Iontrap-MS (Bruker). HPLC parameters were set as follows: solvent A: H_2O + 0.1% formic acid, solvent B: acetonitrile (ACN) + 0.1% formic acid; gradient: 5% B (0.5 min), 5–100% (19.5 min), 100% (5 min), flowrate 0.6 mL/min, and DAD detection 190–600 nm.

HR-ESI-MS spectra were obtained with an Agilent 1200 Infinity Series HPLC (Agilent Technologies, Böblingen, Germany; conditions same as for ESI-MS spectra) connected to a maXis® ESI-TOF-MS (Bruker).

Fungal material and extraction

Approximately 2 g of stromata from chemotype 1 (CT-1) of *Hypoxylon rubiginosum* (I) were used. These were collected in June 2004 from unidentified dead wood in *Parc Natural dels Aiguamolls de l'Empordà*, Catalonia, Spain, by Barbara and Marc Stadler. A specimen of CT-1 is deposited at the herbarium of the Helmholtz Centre for Infection Research (ID: STMA 04057). Stromata of CT-2 ("aberrant"; ca. 6 g) of *H. rubiginosum* (II) were collected by Marc and Benno Stadler in August 2004 from decorticated wood in *Gelpetal*, Wuppertal, Germany, in *Bergisch Nizza* (STMA 04080). For *H. texense* (III), *ca.* 3 g of stromata were collected from *Quercus* wood by Gerald F. Bills in Big Creek, Texas, USA, in January 2020 (STMA 20002).

Extraction of stromatal materials (I)–(III) was performed by adding 500 mL acetone each, followed by ultrasonication at 40 °C for 1 h. This procedure was repeated once. The respective extracts were combined and dried *in vacuo*, which led to the following yields: (I): *ca.*160 mg, (II): *ca.* 620 mg, (III): *ca.* 350 mg. Samples of these crude extracts were subjected to HPLC-MS analysis (Figure S1). The gained HPLC fingerprints were used for chemotaxonomic analysis. This was utilised for species determination along with morphologic characters of the stromatal material.

In order to remove fatty acids and other lipophilic compounds, (I)–(III) were individually pre-fractionated using a Strata-X® C18-E cartridge (10 g/60 mL, SN: 8B-S001-HCH-T, Phenomenex, Torrance, CA/USA). The extracts were dissolved in *ca.* 10 mL of acetone: acetonitrile (ACN) 1:1 and transferred onto the cartridge. Then, a two step-gradient of 20 mL of acetone followed by 20 mL of dichloromethane (DCM) was applied using a vacuum of *ca.* 800 mbar. The eluents of both gradient steps were individually dried *in vacuo*. After HPLC-MS analysis, the acetone fraction of each separation was further processed as described below. Yields were (I): 148 mg, (II): 574 mg, and (III): 300 mg.

Isolation of secondary metabolites 1, 3–7, 9–10, and 13

The isolation of **3** and **5** from (I), **6** and **9**–**10** from (II), as well as **1**, **4**, **7**, and **13** from (III) is described in the following paragraphs. If several injections of the same sample were done, respective fractions containing the same peaks were combined after HPLC-MS analysis. Solvents for all following chromatographic separations were A: H_2O + 0.1% formic acid and B: ACN + 0.1% formic acid.

The acetone fraction of (I) (1×148 mg, dissolved in 10 mL acetone:ACN:H_2O 2:1:1) was separated using a PLC 2250 HPLC system (Gilson, Middleton, WI/USA) equipped with a Gemini C18 column (250×50 mm, 10 μm; Phenomenex) at a flow rate of 60 mL/min and the following gradient: 30% B (5 min), 30–45% (1 min), 45–55% (54 min), 55–100% (20 min), 100% (20 min). This led to the following pure compounds: rubiginosin Y **5** (1.5 mg, t_R: 76–77 min) and rubiginosin C **3** (10.7 mg, t_R: 84–84.5 min).

The acetone fraction of (II) (2×287 mg, each in 10.5 mL acetone:ACN:H_2O 2:1:1) was further processed by injecting twice into the aforementioned PLC 2250 system. The same column and flow rate, but a differing gradient was used: 30% B (5 min), 30–40% (1 min), 40–50% (39 min), 50–100% (25 min), 100% (20 min). This led to the following fractions and pure compounds: fraction (II-a) (9.7 mg, t_R: 60.5–61.5 min), rutilin B **10** (10.3 mg, t_R: 61.5–62.5 min), and fraction (II-b) (23 mg, t_R: 71–72.5 min).

Fraction (II-a) (1×9.7 mg, in 1.5 mL ACN:H_2O 3:1) was further processed using the PLC 2250 system with an X-Bridge C18 column (250×19 mm, 5 μm, Waters) with a flow rate of 20 mL/min. The following gradient was used: 30% B (5 min), 30–52% (5 min), 52–66% (35 min), 66–100% (5 min), 100% (10 min). This yielded rutilin A **9** (3.9 mg, t_R: 24–25 min).

Fraction (II-b) (2×11.5 mg, each in 1.5 mL ACN:H_2O 2:1) was separated using the same conditions as for fraction (I) except for a differing gradient: 30% B (5 min), 30–70% (5 min), 70–80% (40 min), 80–100% (5 min), 100% (10 min). This gave rise to rubiginosin X **6** (6.2 mg, t_R: 32.5–34 min).

The acetone fraction of (III) (1×300 mg, in 15 mL acetone:ACN:H_2O 4:5:1) was separated using the same PLC 2250 system, Gemini C18 column, and flow rate as utilised for (I). The following gradient was applied: 30% B (5 min), 30–40% (10 min), 40–60% (45 min), 60–100% (10 min), 100% (10 min). This led to the following fractions and pure compounds: fraction (III-a) (54 mg, t_R: 25–34.5 min) and rubiginosin W **7** (7.1 mg, t_R: 78.5–80 min).

Fraction (III-a) (4×13.5 mg, each in 0.4 mL acetone:ACN:H_2O 4:1:1) was further purified by quadruple injection using the same conditions as used for fraction (II-a), but a different gradient: 5% B (5 min), 5–40% (5 min), 40–45% (40 min), 45–100% (10 min), 100% (10 min). This led to the following fractions and pure compounds: rubiginosin A **1** (5.6 mg, t_R: 21–22 min), fraction (III-b) (12.5 mg, t_R: 22.5–23.5 min), and mitorubrinol acetate **13** (7.6 mg, t_R: 24.5–26 min).

Fraction (III-b) (1×12.5 mg, in 0.9 mL of acetone:ACN:H_2O 2:1:1) was further processed using the same conditions as above, but a differing gradient: 5% B (5 min), 5–40% (5 min), 40% (30 min), 40–100% (5 min), 100% (10 min). This yielded the pure compound rubiginosin Z **4** (10.6 mg, t_R: 22–24.5 min).

Physicochemical data of rubiginosins Z-W 4–7

Rubiginosin Z **4**: yellow oil; $[\alpha]_D$: +180 (*c* 0.02, MeOH); ^{1}H NMR (acetone-d_6, 700 MHz): see Table S1; ^{13}C NMR (acetone-d_6, 175 MHz): see Table S2; IR (ATR): ν_{max}: 2979, 2936, 2857, 1713, 1643, 1618, 1534 cm^{-1}, see Figure S39; UV/vis (MeOH): λ_{max} (ε): 217 (4.46), 262

(4.06), 304 (3.74), 381 (4.04) nm, see Figure S40; ECD (MeOH) $\lambda(\triangle\varepsilon)$: 210 (−22.2), 224 (+37.7), 244 (+11.3), 262 (+35.2), 296 (−4.8), 336 (+11.8) nm, see Figure S34; ESI-MS: *m/z* 445.13 $[M+H]^+$, 443.09 $[M-H]^-$; HR-ESI-MS: *m/z* 445.1493 $[M+H]^+$ (calcd. for $C_{23}H_{25}O_9$, 445.1498); t_R: 8.9 min.

Rubiginosin Y **5**: red oil; $[\alpha]_D$: +95 (*c* 0.02, MeOH); ^{1}H NMR (acetone-d_6, 700 MHz): see Table S1; ^{13}C NMR (acetone-d_6, 175 MHz): see Table S2; IR (ATR): ν_{max}: 2927, 2855, 1707, 1619, 1591 cm^{-1}, see Figure S39; UV/vis (MeOH): λ_{max} (ε): 218 (4.40), 287 (4.28), 331 (4.22) nm, see Figure S40; ECD (MeOH) $\lambda(\triangle\varepsilon)$: 222 (+8.0), 246 (−0.2), 253 (+1.4), 292 (−5.3), 350 (+12.9) nm, see Figure S34; ESI-MS: *m/z* 485.27 $[M+H]^+$, 483.28 $[M-H]^-$; HR-ESI-MS: *m/z* 485.2538 $[M+H]^+$ (calcd. for $C_{28}H_{37}O_7$, 485.2534); t_R: 13.3 min.

Rubiginosin X **6**: red oil; $[\alpha]_D$: +140 (*c* 0.02, MeOH); ^{1}H NMR (acetone-d_6, 500 MHz): see Table S1; ^{13}C NMR (acetone-d_6, 125 MHz): see Table S2; IR (ATR): ν_{max}: 2957, 2925, 2855, 1695, 1668, 1635, 1609 cm^{-1}, see Figure S39; UV/vis (MeOH): λ_{max} (ε): 217 (4.36), 320 (4.65) nm, see Figure S40; ECD (MeOH) $\lambda(\triangle\varepsilon)$: 215 (+1.7), 221 (+6.3), 250 (−2.0), 271 (−15.0), 297 (+5.2), 318 (−11.2), 349 (+38.6) nm, see Figure S34; ESI-MS: *m/z* 469.21 $[M+H]^+$, 467.29 $[M-H]^-$; HR-ESI-MS: *m/z* 469.2584 $[M+H]^+$ (calcd. for $C_{28}H_{37}O_6$, 469.2592); t_R: 15.2 min.

Rubiginosin W **7**: red oil; $[\alpha]_D$: +85 (*c* 0.02, MeOH); ^{1}H NMR (acetone-d_6, 500 MHz): see Table S1; ^{13}C NMR (acetone-d_6, 125 MHz): see Table S2; IR (ATR): ν_{max}: 2925, 2855, 1717, 1623 cm^{-1}, see Figure S39; UV/vis (MeOH): λ_{max} (ε): 249 (4.01), 291 (4.07), 351 (4.14) nm, see Figure S40; ECD (MeOH) $\lambda(\triangle\varepsilon)$: 215 (−5.8), 248 (+2.4), 285 (−1.5), 367 (+4.8) nm, see Figure S34; ESI-MS: *m/z* 459.31 $[M+H]^+$, 457.28 $[M-H]^-$; HR-ESI-MS: *m/z* 459.2744 $[M+H]^+$ (calcd. for $C_{27}H_{39}O_6$, 459.2745); t_R: 16.1 min.

Mosher's analyses of rubiginosins C 3, Z 4, and W 7

For the preparation of the (*S*)-MTPA ester 0.5 mg of rubiginosin C **3** was dissolved in 250 µL of pyridine-d_5, and 10 µL of (*R*)-MTPA chloride was added. The mixture was incubated at ambient temperature for 15 min and ^{1}H NMR, ^{1}H/^{1}H COSY, ^{1}H/^{13}C HSQC, and ^{1}H/^{13}C HMBC spectra were measured. ^{1}H NMR (700 MHz, pyridine-d_5): similar to **3**,[13] but δ_H 2.81 (11-H_2), 1.33 (13′-H_3) ppm. The (*R*)-MTPA ester was prepared in the same manner by addition of 10 µL of (*S*)-MTPA chloride: ^{1}H NMR (700 MHz, pyridine-d_5): similar to **3**,[13] but δ_H 2.75 (11′-H_2), 1.40 (13′-H_3) ppm. Results are depicted in Figure S31.

Rubiginosin Z **4** (2×0.5 mg) was converted analogously. (*S*)-MTPA ester of **4**: ^{1}H NMR (700 MHz, pyridine-d_5): similar to **4**, but δ_H 3.00/2.89 (6-H_2), 1.65 (11-H_3) ppm. (*R*)-MTPA ester of **4**: ^{1}H NMR (700 MHz, pyridine-d_5): similar to **4**, but δ_H 3.08 (6-H_2), 1.64 (11-H_3) ppm. Results are depicted in Figure S32.

Rubiginosin W **7** (2×0.5 mg) was converted analogously. (*S*)-MTPA ester of **7**: ^{1}H NMR (700 MHz, pyridine-d_5): similar to **7**, but δ_H 3.34 (2′-H), 2.09 (4′-H), 1.35 (5′-H_2), 1.40 (13′-H_3), 1.05 (14′-H_3) ppm. (*R*)-MTPA ester of **7**: ^{1}H NMR (700 MHz, pyridine-d_5): similar to **7**, but δ_H 3.34 (2′-H), 1.99 (4′-H), 1.31/1.08 (5′-H_2), 1.43 (13′-H_3), 0.83 (14′-H_3) ppm. Results are depicted in Figure S33.

Molecular modelling studies of rubiginosins A 1 and Z 4

Rubiginosin A **1** and Z **4** were modelled in Spartan (Spartan 18, v1.4.5 (200203), Wavefunction, Irvine, CA/USA). Structures were initially minimised using a molecular mechanics conformer distribution calculation, and lowest energy conformers were then optimised using semi-empirical PM3 calculations to estimate energies. Higher level calculations (Hartree-Fock 6-31G* and density functional wB97X-D 6-31G*) confirmed the initial observations. Results are depicted in Figure S38.

Bioassays

Minimum inhibitory concentrations (MIC) were determined as described previously.[27] Various test organisms of fungal and bacterial origin were tested. Bacteria: *Bacillus subtilis* (DSM10), *Staphylococcus aureus* (DSM346), *Acinetobacter baumanii* (DSM30008), *Chromobacterium violaceum* (DSM30191), *Escherichia coli* (DSM1116), *Pseudomonas aeruginosa* (PA14); mycobacteria: *Mycolicibacterium smegmatis* (ATCC700084); fungi: *Candida albicans* (DSM1665), *Schizosaccharomyces pombe* (DSM70572), *Mucor hiemalis* (DSM2656), *Pichia anomala* (DSM6766), *Rhodotorula glutinis* (DSM10134). Results are depicted in Table S4.

The cytotoxicity assay against mouse fibroblast cell line L929 as well as human cervical cancer cell line KB 3.1 was performed as described before.[27] If half-maximum inhibitory concentration (IC_{50}) values smaller than 10 µM were observed, additional cell lines were subjected to the azaphilones: PC-3, SK-OV-3, MCF-7, A431, and A549. Results are depicted in Table 1.

Bioinformatic analysis for gene cluster prediction

The genome of the ex-epitype *H. rubiginosum* strain MUCL 52887 was sequenced by using PacBio, and gene prediction and annotation were carried out as previously described.[28] Candidate biosynthetic gene clusters (BGCs) were manually identified by BLASTp searches using Hfaza1A (QNC49737) and Hfaza2A (QNC49725) as template against a created *H. rubiginosum* protein database. The searches were performed with the software Geneious 9.1.8 (https://www.geneious.com). Homology between related BGCs was mapped and visualized with the clinker tool.[26] The identified gene clusters were uploaded to GenBank under the accession numbers MW296097 (*hraza1*) and MW296098 (*hraza2*).

Acknowledgements

Foremost, the authors would like to thank Marc Stadler for generous support of this work. The authors wish to thank Silke Reinecke for expert assistance in the lab. We are also grateful for the help of Esther Surges for recording the HR-ESI-MS spectra, as well as Christel Kakoschke for performing the NMR measurements. K. Becker, E. Kuhnert, and R. J. Cox are grateful for a grant from the Deutsche Forschungsgemeinschaft (DFG CO 1328/4-1) in the Priority Programme "Taxon-Omics: New Approaches for Discovering and Naming Biodiversity" (SPP 1991). Open Access funding enabled and organized by Projekt DEAL.

Conflict of Interest

The authors declare no conflict of interest.

Keywords: Biosynthesis · Hypoxylaceae · Pigments · Polyketides · Xylariales

[1] a) F. P. Coyne, H. Raistrick, R. Robinson, *Philos. Trans. R. Soc. London Ser. A* **1931**, *220*, 297–300; b) Y. He, R. J. Cox, *Chem. Sci.* **2016**, *7*, 2119–2127.
[2] a) C. Chen, H. Tao, W. Chen, B. Yang, X. Zhou, X. Luo, Y. Liu, *RSC Adv.* **2020**, *10*, 10197–10220; b) J. M. Gao, S. X. Yang, J. C. Qin, *Chem. Rev.* **2013**, *113*, 4755–4811.
[3] W. Steglich, M. Klaar, W. Furtner, *Phytochemistry* **1974**, *13*, 2874–2875.
[4] D. N. Quang, T. Hashimoto, M. Stadler, Y. Asakawa, *Tetrahedron* **2005**, *61*, 8451–8455.
[5] a) D. N. Quang, T. Hashimoto, Y. Nomura, H. Wollweber, V. Hellwig, J. Fournier, M. Stadler, Y. Asakawa, *Phytochemistry* **2005**, *66*, 797–809; b) D. N. Quang, M. Stadler, J. Fournier, A. Tomita, T. Hashimoto, *Tetrahedron* **2006**, *62*, 6349–6354; c) F. Surup, K. I. Mohr, R. Jansen, M. Stadler, *Phytochemistry* **2013**, *95*, 252–258.
[6] E. Kuhnert, F. Surup, E. B. Sir, C. Lambert, K. D. Hyde, A. I. Hladki, A. I. Romero, M. Stadler, *Fungal Divers.* **2015**, *71*, 165–184.
[7] a) T. Hashimoto, S. Tahara, S. Takaoka, M. Tori, Y. Asakawa, *Chem. Pharm. Bull.* **1994**, *42*, 2397–2399; b) D. N. Quang, T. Hashimoto, M. Tanaka, M. Stadler, Y. Asakawa, *Phytochemistry* **2004**, *65*, 469–473.
[8] L. Wendt, E. B. Sir, E. Kuhnert, S. Heitkämper, C. Lambert, A. I. Hladki, A. I. Romero, J. J. Luangsa-ard, P. Srikitikulchai, D. Peršoh, M. Stadler, *Mycol. Prog.* **2018**, *17*, 115–154.
[9] a) F. Surup, A. Narmani, L. Wendt, S. Pfütze, R. Kretz, K. Becker, C. Menbrivès, A. Giosa, M. Elliott, C. Petit, M. Rohde, M. Stadler, *Fungal Divers.* **2018**, *92*, 345–356; b) K. Becker, S. Pfütze, E. Kuhnert, R. J. Cox, M. Stadler, F. Surup, *Chem. Eur. J.* **2021**, *27*, 1438–1450.
[10] D. Wibberg, M. Stadler, C. Lambert, B. Bunk, C. Spröer, C. Rückert, J. Kalinowski, R. J. Cox, E. Kuhnert, *Fungal Divers.* **2020**, *106*, 7–28.
[11] E. Kuhnert, J. C. Navarro-Muñoz, K. Becker, M. Stadler, J. Collemare, R. J. Cox, *Stud. Mycol.* 2021, 99, 100118 DOI: 10.1016/j.simyco.2021.100118.
[12] M. Stadler, J. Fournier, A. Granmo, E. Beltrán-Tejera, *N. Am. Fungi* **2008**, *3*, 73–125.
[13] D. N. Quang, T. Hashimoto, M. Stadler, Y. Asakawa, *J. Nat. Prod.* **2004**, *67*, 1152–1155.
[14] S. Halecker, J.-P. Wennrich, S. Rodrigo, N. Andrée, L. Rabsch, C. Baschien, M. Steinert, M. Stadler, F. Surup, B. Schulz, *Fungal. Ecol.* **2020**, *45*, 100918.
[15] E. B. Sir, K. Becker, C. Lambert, G. F. Bills, E. Kuhnert, *Mycologia* **2019**, *111*, 832–856.
[16] Y. X. Yang, J. X. Wang, Q. Wang, H. L. Li, M. Tao, Q. Luo, H. Liu, *Fitoterapia* **2018**, *127*, 396–401.
[17] M. Stadler, H. Wollweber, J. Fournier, *Mycotaxon* **2004**, *90*, 187–211.
[18] T. R. Hoye, C. S. Jeffrey, F. Shao, *Nat. Protoc.* **2007**, *2*, 2451–2458.
[19] R. C. Clark, S. Y. Lee, D. L. Boger, *J. Am. Chem. Soc.* **2008**, *130*, 12355–12369.
[20] N. Matsumori, D. Kaneno, M. Murata, H. Nakamura, K. Tachibana, *J. Org. Chem.* **1999**, *64*, 866–876.
[21] K. Furihata, H. Seto, *Tetrahedron Lett.* **1999**, *40*, 6271–6275.
[22] W. Koźmiński, D. Nanz, *J. Magn. Reson.* **1997**, *124*, 383–392.
[23] J. Chen, J. Li, L. Wu, Y. Geng, J. Yu, C. Chong, M. Wang, Y. Gao, C. Bai, Y. Ding, Y. Chen, Q. Zhang, *Eur. J. Med. Chem.* **2018**, *151*, 601–627.
[24] L. Q. Li, Y. G. Yang, Y. Zeng, C. Zou, P. J. Zhao, *Molecules* **2010**, *15*, 3993–3997.
[25] a) M. Stadler, J. Fournier, D. N. Quang, A. Y. Akulov, *Nat. Prod. Commun.* **2007**, *2*, 223–350; b) M. Stadler, D. N. Quang, A. Tomita, T. Hashimoto, Y. Asakawa, *Mycol. Res.* **2006**, *110*, 811–820.
[26] C. L. M. Gilchrist, Y. H. Chooi, *Bioinformatics* **2021**, *37*, 2473–2375.
[27] K. Becker, A. C. Wessel, J. J. Luangsa-Ard, M. Stadler, *Biomol. Eng.* **2020**, *10*, 805.
[28] C. Wang, K. Becker, S. Pfütze, E. Kuhnert, M. Stadler, R. J. Cox, E. Skellam, *Org. Lett.* **2019**, *21*, 8756–8760.

Manuscript received: December 28, 2020
Revised manuscript received: July 17, 2021
Accepted manuscript online: July 19, 2021